Inorganic Chemistry

ARTICLE

pubs.acs.org/IC

Electronic Structures and Spectroscopy of the Electron Transfer Series $[Fe(NO)L_2]^z$ (z = 1+, 0, 1−, 2−,3−; L = Dithiolene)

Panida Surawatanawong,[†,‡] Stephen Sproules,[†,§] Frank Neese,*[,†,∥] and Karl Wieghardt*[,†]

[†]Max-Planck-Institut für Bioanorganische Chemie, Stiftstrasse 34-36, D-45470 Mülheim an der Ruhr, Germany

[§]EPSRC National UK EPR Facility and Service, Photon Science Institute, The University of Manchester, Oxford Road, Manchester M13 9PL, U.K.

[∥]Institut für Physikalische und Theoretische Chemie, Universität Bonn, Wegelerstrasse 12, D-53115 Bonn, Germany

Supporting Information

ABSTRACT: The electronic structures and spectroscopic parameters for the electron transfer series of $[Fe(NO)(L)_2]^z$ (z = 1+, 0, 1−, 2−, 3−; L = $S_2C_2R_2$; R = *p*-tolyl (**1**) and CN (**2**)) were calculated and compared to experiment. Some compounds in the series were isolated and characterized by spectroscopy. The calculations support the notion that all the monocation ($S_t = 0$), neutral ($S_t = {}^1/_2$), and monoanion ($S_t = 0$) complexes contain NO^+ ($S_{NO} = 0$), in which the redox active fragment is either the bis-dithiolene (2 L) or the central iron. The calculated electronic structures give insight into how *p*-tolyl and CN substituents and the redox states of the 2 L ligand impact the spin density on the iron in the monocation and neutral species. The electronic structure of $[\mathbf{1}]^0$ has some $[Fe^I(NO^+)(L_2^{2-})]^0$ character in resonance with $[Fe^{II}(NO^+)(L_2^{2-})]^0$ whereas $[\mathbf{2}]^0$ has a smaller amount of a $[Fe^I(NO^+)(L_2^{2-})]^0$ description in its ground state wavefunction. Similarly, the electronic structure of $[\mathbf{1}]^{1+}$ also has some $[Fe^I(NO^+)(L_2^{1-})]^{1+}$ character in resonance with $[Fe^{II}(NO^+)(L_2^{2-})]^{1+}$ whereas $[\mathbf{2}]^{1+}$ is best described as $[Fe^{II}(NO^+)(L^{\bullet})_2]^{1+}$. For the monoanion, the bis-dithiolene fragment is fully reduced and both $[\mathbf{1}]^-$ and $[\mathbf{2}]^-$ are best formulated as $[Fe^{II}(NO^+)(L_2^{4-})]^-$. The reduction of the monoanion to give dianions $[\mathbf{1}]^{2-}$ and $[\mathbf{2}]^{2-}$ results in $\{FeNO\}^7$ species. The calculated ^{57}Fe isomer shift and hyperfine couplings are in line with the experiment and support a description of the form $[Fe^{III}(NO^-)(L_2^{4-})]^{2-}$, in which Fe(III) $S_{Fe} = {}^3/_2$ is antiferromagnetically coupled to NO^- ($S_{NO} = 1$). Finally, the calculated redox potential and ν(NO) frequency for the $\{FeNO\}^8$ trianionic species $[\mathbf{2}]^{3-}$ is in agreement with experiment and consistent with a triplet ground state $[Fe^{II}(NO^-)(L_2^{4-})]^{3-}$, in which Fe(II) ($S_{Fe} = 2$) is involved in antiferromagnetic coupling with NO^- ($S_{NO} = 1$).

INTRODUCTION

Metal(bis-dithiolene) complexes have been subject of intense studies due to the noninnocent nature of the dithiolene ligand.[1] Attention has been given to the electrochemically controlled ligand binding and release of small molecules. Stiefel and co-workers reported that $Ni(S_2C_2(CF_3)_2)_2$ could be used for the olefin separation from a multicomponent sample.[2] Donahue and co-workers reported that Fe(bis-dithiolene) can bind and release triphenylphosphine reversibly upon reduction or oxidation.[3] Understanding the electronic structures of the metal(bis-dithiolene) complexes in the electron transfer series should assist in understanding and further developing of these applications.

McCleverty and co-workers,[4] have reported an electron transfer series $Fe(NO)(mnt)_2$ (mnt^{2-} = maleonitriledithiolate). However, the electronic structures of this series of compounds have not been studied in detail. Recently, an analogous electron transfer series based on Fe(NO)(bis-dithiolene) has been isolated and spectroscopically characterized by Wieghardt and co-workers.[5] However, this system is electronically highly complex. Unlike homoleptic Fe(bis-dithiolene) with two redox-active fragments, Fe(NO)(bis-dithiolene) has *three* redox-active sites: (1) the central iron, (2) the nitrosyl ligand, and (3) the dithiolene ligands.[6] The question arises in which order redox events take place. To answer this intriguing fundamental question in the coordination chemistry of noninnocent ligands, it is crucial to determine the oxidation state of the central iron,[5] though this is known to be a nontrivial exercise for iron-nitrosyl complexes. According to the notation introduced by Feltham and Enemark, the complexes are denoted as $\{FeNO\}^n$, in which n is the sum of the number of electrons in the Fe d orbitals and the number of electrons in the nitrosyl π^* orbitals.[7] From previous spectroscopic studies of the electron transfer series $[Fe(NO)(L)_2]^z$, where z = 1+, 0, 1−, 2−, and L = $S_2C_2R_2$ for R = *p*-tolyl (**1**), CN (**2**), the monocationic ($S_t = 0$), neutral ($S_t = {}^1/_2$), and monoanionic ($S_t = 0$) species were proposed to be $\{FeNO\}^6$ complexes, in which the dithiolene ligand is the redox active site, while the dianion ($S_t = {}^1/_2$) and trianion (electrochemically observed for complex **2** though the spin ground state was not

Received: July 21, 2011
Published: November 03, 2011

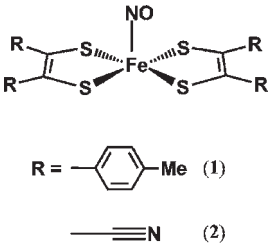

Figure 1. Complexes.

reported) are expected to be $\{FeNO\}^7$ and $\{FeNO\}^8$ species, respectively.[5]

In this study, broken symmetry density functional theory (BS-DFT) is applied to elucidate the electronic structure of each species in the electron transfer series of compounds **1** and **2** in detail (Figure 1). In order to come to valid conclusions, we have calculated various spectroscopic parameters and compared them to both new and existing experimental data.

COMPUTATIONAL DETAILS

The program package ORCA was used for all calculations.[8] Geometry optimization and frequency calculations were carried out using the B3LYP[9]/BS-I (and, as discussed below, BP86[10] in some $\{FeNO\}^7$ species). Basis set I (BS-I) consists of TZVP[11] for Fe, S, N, and O atoms and SV(P)[12] for C and H. The zeroth-order regular approximation (ZORA) has been used in the geometry optimizations.[13] Auxiliary basis sets for all complexes used to expand the electron density in the calculations were chosen to match the orbital basis. The self-consistent field (SCF) calculations were tightly converged (1×10^{-8} E_h in energy, 1×10^{-7} E_h in the density change, and 1×10^{-7} in the maximum element of the DIIS[14] error vector). The geometry search for all complexes was carried out in redundant internal coordinates without imposing geometry constraints. Initial coordinates for $[\mathbf{1}]^0$,[5] $[\mathbf{1}]^-$,[5] $[\mathbf{2}]^-$,[15] and $[\mathbf{2}]^{2-}$,[16,17] $[\mathbf{3}]^-$,[18] $[\mathbf{3}]^{2-}$,[19] and $[\mathbf{4}]^0$,[20] were obtained from their crystal structures. For the other members of each series, $[\mathbf{1}]^{1+}$ was optimized starting from the crystal structure coordinates of $[\mathbf{1}]^0$; $[\mathbf{1}]^{2-}$ from $[\mathbf{1}]^-$; $[\mathbf{2}]^{1+}$ and $[\mathbf{2}]^0$ from $[\mathbf{2}]^-$; and $[\mathbf{2}]^{3-}$ from $[\mathbf{2}]^{2-}$. The optimized coordinates are posted in the Supporting Information. Optimized geometries are used for all computed Mössbauer parameters[21,22] at the B3LYP/BS-II level. BS-II consists of CP(PPP)[21] for Fe and is otherwise identical to BS-I. Mössbauer isomer shifts and quadrupole splittings are calculated as described earlier.

The reduction potential ($E°$) vs ferrocene/ferrocenium (Fc/Fc^+) couple was calculated for the electron transfer series of complex **2**. The details of this calculation are explained elsewhere.[23] The solvation free energy in CH_2Cl_2 ($\varepsilon = 9.08$) was calculated using B3LYP/BS-III on the gas phase optimized geometries of complex $[\mathbf{2}]^z$ by using the COSMO continuum solvation method.[24] In BS-III, the CP(PPP) basis set was used for Fe, and TZVP was used for all other atoms.

BS calculations make use of the notation BS(m,n)[25] using the method of Noodleman and co-workers.[26] We adopted the following notation: the given system was divided into two fragments. The notation BS(m,n) refers then to a broken symmetry state with m unpaired α-spin electrons essentially on fragment 1 and n unpaired β-spin electrons localized on fragment 2. In most cases, fragments 1 and 2 correspond to the metal and the ligands, respectively. In this notation, the standard high-spin, open-shell solution is written as BS($m + n$,0). The BS(m,n) notation refers to the initial guess to the wave function. The variational process does, however, have the freedom to converge to a solution of the form BS($m - n$,0), in which effectively the n β-spin electrons pair up with $n < m$ α-spin electrons on the partner fragment. Such a solution is then a standard $M_S \cong (m - n)/2$ spin-unrestricted Kohn−Sham solution. As explained elsewhere,[27] the nature of the solution is investigated from the corresponding orbital transformation (COT), which, from the corresponding orbital overlaps, displays whether the system should be described as a spin-coupled or a closed-shell solution. For the BS calculations, the MO schemes are plotted for the spin-coupled and singly occupied orbitals from the corresponding orbitals,[27] whereas, for the doubly occupied and unoccupied orbitals, they are represented by quasi-restricted orbitals (QROs). Canonical orbitals are plotted for the standard spin-restricted closed-shell calculation (they coincide with QROs). All orbitals were plotted with an isodensity of 0.05 using Jimp2.[28] Löwdin spin populations for the molecular fragments are shown on the spin density plots with an isodensity of 0.003 using Molekel.[29] As discussed many times elsewhere,[25,30] spin densities obtained in BS calculations should be recognized to be unrealistic. However, their virtue lies in providing an effective means of visualizing the density of unpaired electrons in the system in an easy way to grasp.

RESULTS AND DISCUSSION

1. Geometric and Electronic Structures of 1 and 2. *a. [Fe(NO)(L$_2$)]^0.* The BS solutions, BS(2,1) and BS(3,2), and the non-BS spin-unrestricted solution (alternatively referred to as BS(1,0)) were calculated for the neutral complex $[\mathbf{1}]^0$. The optimized geometric parameters in comparison to the X-ray crystal structure[5] are shown in Table S1 of the Supporting Information. The Fe−NO bond distances from BS(3,2) are overestimated by 0.1 Å. The non-BS spin-unrestricted calculation gives the same solution as the BS(2,1) solution. The BS(2,1) solution is not only more stable than BS(3,2) but also has geometric parameters in good agreement with the experimental structure determined by X-ray crystallography (Table 1). Slightly overestimated bond distances (~0.05 Å) are typical for the B3LYP functional.[31] Although there is no X-ray crystal structure available for $[\mathbf{2}]^0$, the non-BS calculation also gives the same solution as the BS(2,1) solution; it is also more stable than BS(3,2), and we will discuss the BS(2,1) solution of $[\mathbf{2}]^0$ in comparison to $[\mathbf{1}]^0$.

From the MO scheme for $[\mathbf{1}]^0$ (Figure 2, top), three doubly occupied Fe d orbitals are the $d_{x^2-y^2}$ nonbonding and d_{yz} and d_{xz} bonding with π_y^* and π_x^* of NO. The singly occupied molecular orbital (SOMO) is dithiolene-based with b_1 symmetry. One spin-coupled pair is found between the Fe d_{z^2} orbital and the dithiolene-based a_1 orbital, and the large spatial overlap integral ($S = 0.81$) highlights the strength of this interaction. The calculated spin population of $[\mathbf{1}]^0$ (Figure 2, bottom) shows a significant amount of spin population on Fe (−1.23) and bis-dithiolene (1.60) as well as some spin also on the nitrosyl ligand (0.63). The spin density calculated on the central Fe derives from the d_{z^2} orbital involved in spin-coupling with the a_1 bis-dithiolene orbital. Spin density on the NO fragments results from polarization of the Fe−NO π^* bonds, which are endowed with significant NO character (~30%).

Complex $[\mathbf{2}]^0$ also shows a spin-coupled pair between the Fe d_{z^2} orbital and the bis-dithiolene a_1 orbital (Figure 3, top). An even larger spatial overlap ($S = 0.91$) is calculated here, and the spin down orbital has nearly the same amount of Fe (53.3%) and 2L (42.9%) content. The spin populations on the Fe (−0.67) and the nitrosyl (0.29) fragments are also somewhat smaller in corresponding to the smaller degree of spin polarization. This implies that the better electron withdrawing capability of the cyano-substituted ligand of **2** in comparison to the *p*-tolyl

dx.doi.org/10.1021/ic201565d |*Inorg. Chem.* 2011, 50, 12064–12074

Table 1. Selected Bond Distances (Å) and Angles (deg) for $[1]^z$ and $[2]^z$ (z = 1+, 0, 1−)

	$S_t = 0$		$S_t = {}^1/_2$			$S_t = 0$			
	$[1]^{1+}$	$[2]^{1+}$	$[1]^0$		$[2]^0$	$[1]^-$		$[2]^-$	
	calcd	calcd	exptl[a]	calcd	calcd	exptl[a]	calcd	exptl[b]	calcd
Fe−N	1.656	1.633	1.637	1.642	1.621	1.624	1.597	1.612	1.593
Fe−S_{av}	2.240	2.230	2.208	2.258	2.252	2.229	2.258	2.233	2.263
N−O	1.148	1.131	1.165	1.159	1.143	1.176	1.163	1.149	1.152
S−C_{av}	1.705	1.697	1.707	1.728	1.720	1.746	1.765	1.723	1.751
C−C_{av}	1.434	1.423	1.387	1.401	1.398	1.368	1.373	1.379	1.379
Fe−N−O	179.9	179.8	180.0	179.0	179.7	176.2	179.9	180.0	179.9

[a] Reference 5. [b] Reference 15.

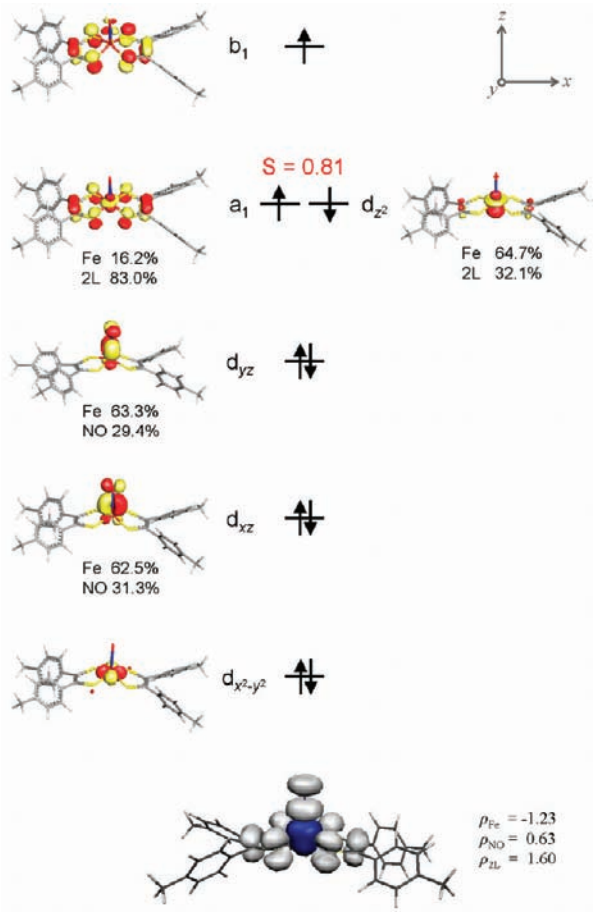

Figure 2. Top: Qualitative MO scheme for $[1]^0$ with contributions from the Fe, NO, and 2L fragments shown for selected orbitals. Bottom: Spin density plot with partial spin populations for Fe, NO, and 2L.

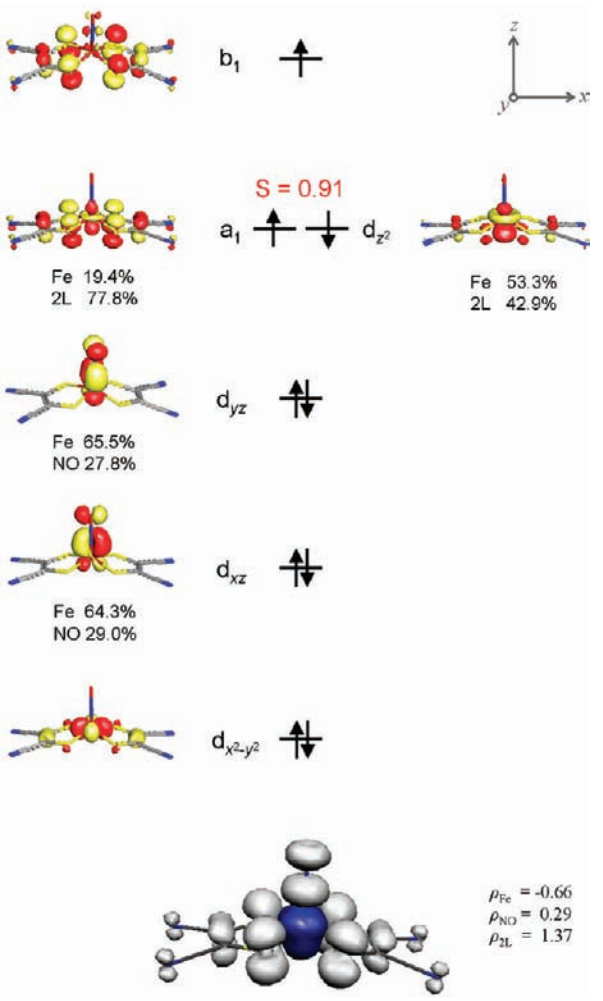

Figure 3. Top: Qualitative MO scheme for $[2]^0$ with contributions from the Fe, NO, and 2L fragments shown for selected orbitals. Bottom: Spin density plot with partial spin populations for Fe, NO, and 2L.

of **1** modulates the extent of delocalization from the bis-dithiolene onto the {FeNO} unit.

Two resonance forms are used to describe the electronic structure for $[1]^0$ and $[2]^0$: (a) Fe(II) ($S_{Fe} = 0$), (L_2^{3-}) ($S_{2L} = {}^1/_2$), and NO^+ ($S_{NO} = 0$), as proposed in the previous work,[5] and (b) Fe(I) ($S_{Fe} = {}^1/_2$) antiferromagnetically coupled with (L_2^{2-}) ($S_{2L} = 1$), and NO^+ ($S_{NO} = 0$). Complex $[1]^0$ is best viewed as an Fe(I) species whereas $[2]^0$ tends more to the low-spin Fe(II) description, as denoted by the smaller spin population on Fe and large spatial overlap of the spin-coupled pair.

b. [Fe(NO)(L_2)]$^{1+}$. While $[2]^{1+}$ is not observed, $[1]^{1+}$ is characterized as a diamagnetic species.[5] Therefore, closed-shell and BS(1,1) calculations were attempted. The BS solution for $[1]^{1+}$ was found to be almost isoenergetic with the closed-shell solution

dx.doi.org/10.1021/ic201565d |*Inorg. Chem.* 2011, 50, 12064–12074

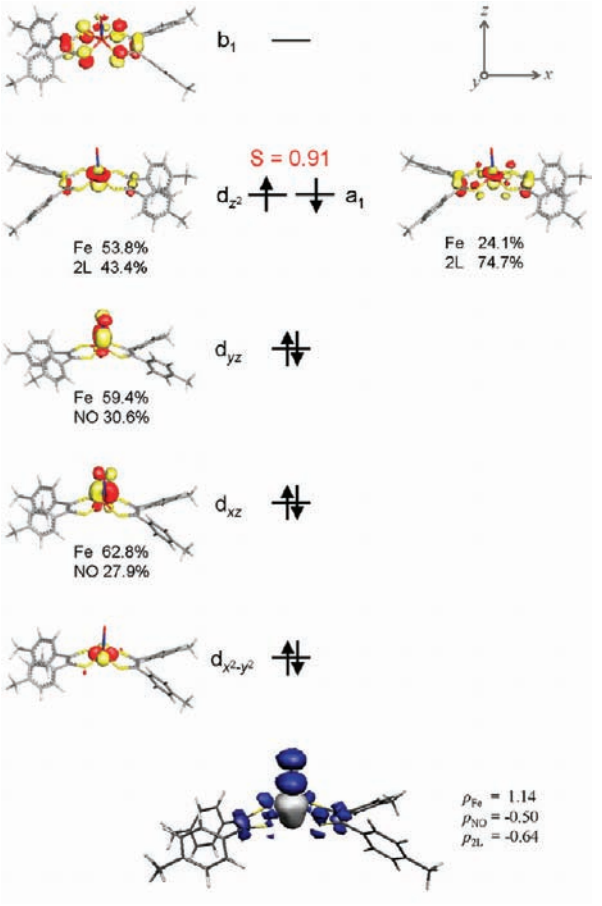

Figure 4. Top: Qualitative MO scheme for $[\mathbf{1}]^{1+}$ with contributions from the Fe, NO, and 2L fragments shown for selected orbitals. Bottom: Spin density plot with spin populations for Fe, NO, and 2L.

(Table S1 of the Supporting Information). The Fe—N and Fe—S bond distances are slightly longer in the BS(1,1) solution than the closed-shell electronic structure. From the MO scheme of $[\mathbf{1}]^{1+}$ (Figure 4), it is seen that oxidation of $[\mathbf{1}]^{0}$ results in removal of one electron from the singly occupied b_1 orbital. A large spatial overlap (S = 0.91) is found between Fe d_{z^2}-based orbital and bis-dithiolene a_1 orbital, with nearly equal contributions from both in the spin-down orbital. Therefore, $[\mathbf{1}]^{1+}$ can also be described by two resonance structures: (a) Fe(II) ($S_{Fe} = 0$), (L_2^{2-}) ($S_{2L} = 0$), and NO^+ ($S_{NO} = 0$), from the closed-shell solution, and (b) Fe(I) ($S_{Fe} = {}^1/_2$) antiferromagnetic coupled with (L_2^{1-}) ($S_{2L} = {}^1/_2$), and NO^+ ($S_{NO} = 0$), from the BS(1,1) solution. The decrease of spin density on the bis-dithiolene moiety by ~0.7 units (Figures 2 and 4) also clearly supports a dithiolene-centered oxidation of $[\mathbf{1}]^{0}$.

In contrast to $[\mathbf{1}]^{1+}$, a BS solution for $[\mathbf{2}]^{1+}$ was not found, since the calculations converged back to the closed-shell state. Three metal-based MOs are doubly occupied although the Fe d_{xz} and d_{yz} orbitals are highly covalent with the NO and bis-dithiolene orbitals (Figure 5). The HOMO contains mainly the bis-dithiolene a_1 orbital with some contribution from the Fe d_{z^2} orbital. Therefore, the electronic structure of $[\mathbf{2}]^{+}$ can simply be described as Fe(II) ($S_{Fe} = 0$), (L_2^{2-}) ($S_{2L} = 0$), and NO^+ ($S_{NO} = 0$).

c. [Fe(NO)(L_2)]$^-$. Reduction of $[\mathbf{1}]^{0}$ and $[\mathbf{2}]^{0}$ sees one electron deposited into the b_1 orbital, resulting in diamagnetic monoanionic

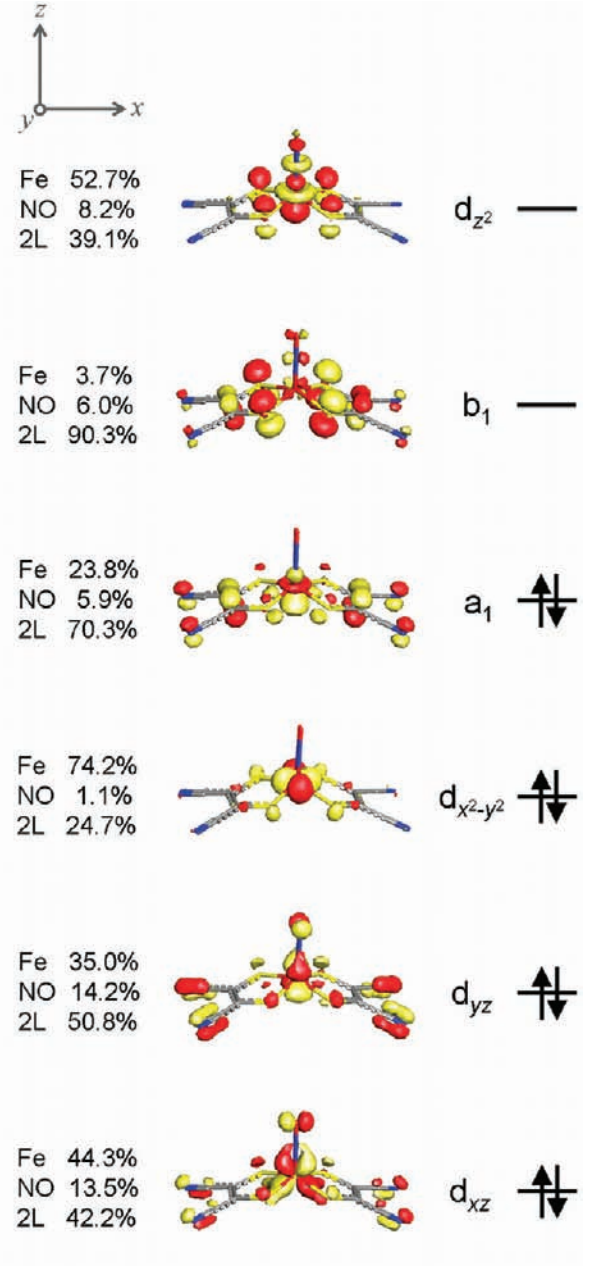

Figure 5. Qualitative MO scheme for $[\mathbf{2}]^{+}$ with contributions from the Fe, NO, and 2L fragments shown.

complexes. The X-ray crystal structures are available for both $[\mathbf{1}]^{-}$ and $[\mathbf{2}]^{-}$.[5,15] The BS(1,1) and BS(2,2) solutions converge to the closed-shell solution with an overlap integral close to unity for both complexes, and the calculated geometric structures are in good agreement with the experiment (Table 1). Canonical orbitals from the spin-restricted closed-shell calculation are shown for $[\mathbf{1}]^{-}$ (Figure 6) and $[\mathbf{2}]^{-}$ (Figure S1 of the Supporting Information). Three metal-based MOs are doubly occupied, with d_{xz} and d_{yz} orbitals lying lower than the $d_{x^2-y^2}$ orbital. The HOMO and HOMO-1 orbitals are dithiolene-based a_1 and b_1 orbitals, and the previously spin-coupled d_{z^2} orbital in $[\mathbf{1}]^{0}$ is now described as empty.

d. Monocation, Neutral, and Monoanion: {FeNO}^{6} Complexes? The calculated electronic structures and geometries in comparison

dx.doi.org/10.1021/ic201565d |*Inorg. Chem.* 2011, 50, 12064–12074

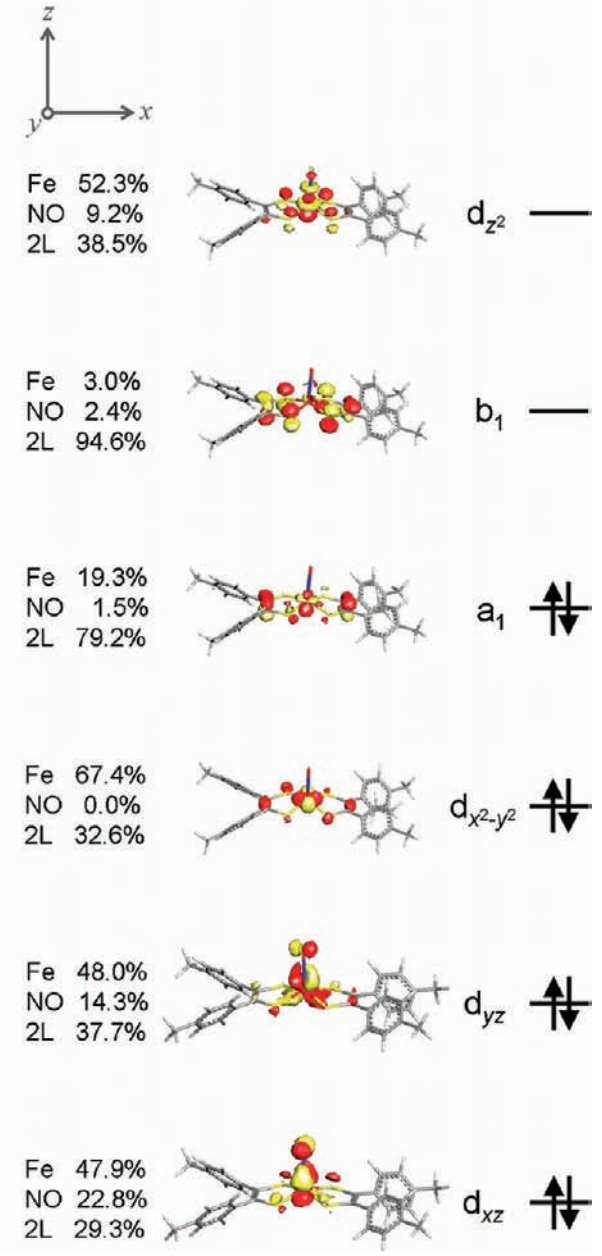

Figure 6. Qualitative MO scheme for $[\mathbf{1}]^-$ with contributions from the Fe, NO, and 2L fragments shown for selected orbitals.

to the X-ray crystal structure support the notion that the electron count on the nitrosyl fragment remains unchanged in the first two-electron transfers of the monocations $[\mathbf{1}]^+$ and $[\mathbf{2}]^+$, as previously proposed.[5] However, the description of the monocation, neutral, and monoanion of **1** and **2** as simple $\{FeNO\}^6$ species demands more justification.

While the monoanion of **1** is undoubtedly a $\{FeNO\}^6$ species, the monocationic and neutral complexes are better described by two resonance structures involving Fe(II) and Fe(I), respectively (Scheme 1)—as $\{FeNO\}^6$ and $\{FeNO\}^7$ species. On the other hand, for **2,** both the monocation and monoanion are $\{FeNO\}^6$ species, whereas the neutral complex can be described by resonance structures involving contributions from $\{FeNO\}^6$ and $\{FeNO\}^7$ moieties. The Fe(I) character in some of these species is represented by the weak antiferromagnetic coupling between

Scheme 1

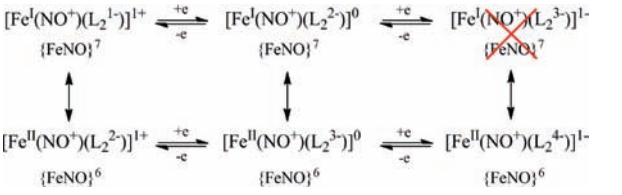

Scheme 2

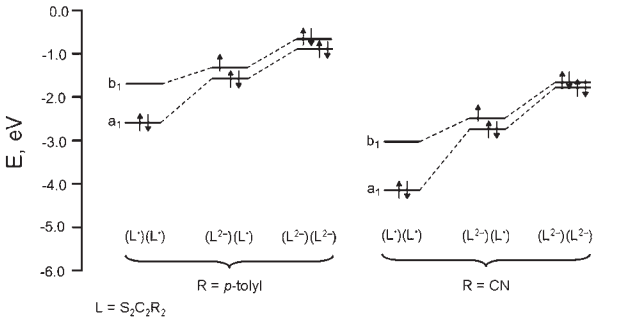

the dithiolene-based a_1 orbital and the Fe d_{z^2}-based orbital, wherein the spatial overlap integral defines the magnitude of the interaction. The discrepancy in the electronic structure descriptions in the reduced forms of **1** and **2** can be rationalized by the calculated relative orbital energies of the dithiolene-based a_1 and b_1 MOs (Scheme 2). The orbital energies of the cyano substituted dithiolene ligand are inherently more stable than their *p*-tolyl counterparts due to the better electron withdrawing ability of the former. The d_{z^2}-based orbital energy is presumably similar to that of the a_1 orbital in the $(L^{2-})(L^{\bullet})$ and $(L^{\bullet})(L^{\bullet})$ units with the *p*-tolyl substituent and in the $(L^{2-})(L^{\bullet})$ fragment with the CN substituent, whereas the a_1 orbital of the $(L^{\bullet})(L^{\bullet})$ fragment with CN is essentially too low. Therefore, the antiferromagnetic coupling between the a_1 MO and the Fe d_{z^2}-based orbital is only found in $[\mathbf{1}]^{1+}$, $[\mathbf{1}]^0$, and $[\mathbf{2}]^0$, but not in $[\mathbf{2}]^{1+}$. The assignment of the monoanion as an Fe(II) complex for both **1** and **2** is based on the fact that the Fe d_{z^2}-based orbital is raised higher in energy than the a_1 MO when the Fe center is moving down toward the equatorial 4S plane in the more reduced species (Figure 7a, vide infra).

Traversing these series from monocation to neutral to monoanion, the S−C bond distances and the C−C bond distances of the dithiolene ligands are seen to significantly increase and decrease (by about 0.02−0.03 Å), respectively, while the N−O bond only marginally lengthens by ∼0.01 Å. The Fe−N distance also decreases upon reduction (Table 1). The change in the S−C and C−C bond distances reflects the addition of electrons into the a_1 and b_1 orbitals, which are antibonding with respect to the S−C bonds and bonding with respect to the C−C bonds, similar to what has been found upon reduction of square planar metal bis-dithiolene compounds.[32] Interestingly, the addition of electrons to a bis-dithiolene orbital not only changes the bond distances within the dithiolene unit, but the Fe−N and N−O bond distances are also mildly affected. Moreover, the Fe center is drawn down toward the 4S equatorial plane, with concomitant shortening of Fe−N. The correlation between the Fe−N bond distance and the distance of Fe to the 4S plane (Fe--4S) for $[\mathbf{1}]^z$ and $[\mathbf{2}]^z$ (z = 1+, 0, 1−) is shown in Figure 7a. Conversely, the

dx.doi.org/10.1021/ic201565d |*Inorg. Chem.* 2011, 50, 12064–12074

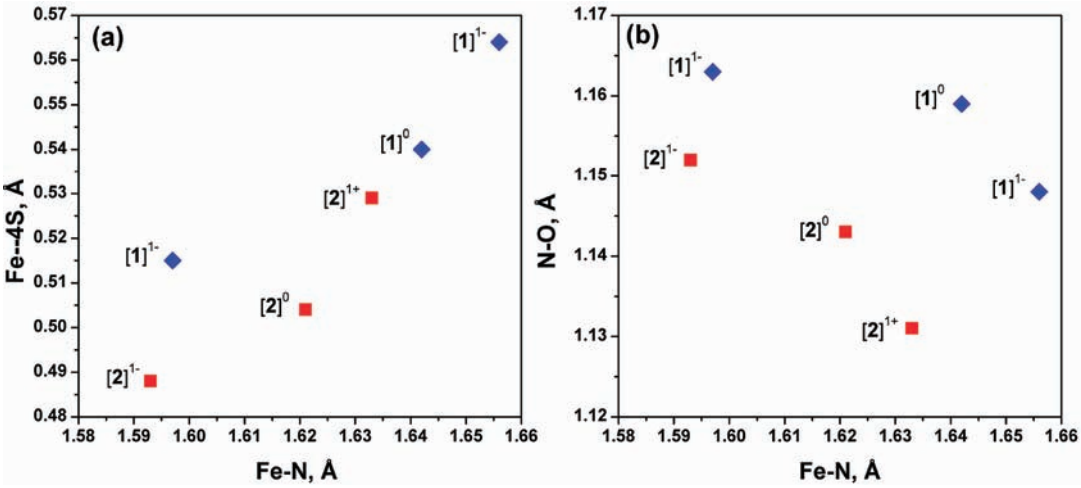

Figure 7. Correlation between calculated Fe−N distance and (a) Fe--4S distance, and (b) N−O distance for $\{FeNO\}^6$ complexes $[\mathbf{1}]^z$ (diamond) and $[\mathbf{2}]^z$ (square), where z = 1+, 0, 1−.

Table 2. Selected Bond Distances (Å) and Angles (deg) for $[\mathbf{1}]^{2-}$ and $[\mathbf{2}]^{2-}$ (S_t = 0)

	$[\mathbf{1}]^{2-}$		$[\mathbf{2}]^{2-}$		
	B3LYP	BP86	exptl[a]	B3LYP	BP86
Fe−N	1.826	1.680	1.721	1.805	1.684
Fe−S_{av}	2.318	2.273	2.266	2.230	2.281
N−O	1.198	1.204	1.148	1.189	1.198
S−C_{av}	1.776	1.777	1.739	1.759	1.765
C−C_{av}	1.378	1.394	1.374	1.383	1.397
Fe−N−O	146.4	149.4	150.9	149.6	149.0

[a] Reference 17.

Fe−N distance is inversely correlated with the N−O bond distance across these series (Figure 7b).

For the more reduced species the electron delocalization from the bis-dithiolene fragment toward the Fe−NO fragment leads to a stronger Fe−N bond and a weaker N−O bond. In analogy to the effect of porphyrin substituents on the reactivity of the NO in FeNO−heme complexes,[33] here the change in NO bond strength upon reduction of the bis-dithiolene unit suggests that the reactivity of axially coordinated NO ligands could be modulated by controlled electrochemical reduction of the noninnocent equatorial ligands.

e. [Fe(NO)(L$_2$)]$^{2-}$. One-electron reduction of the monoanions barely alters the S−C and C−C bond distances, whereas the Fe−N and N−O bonds are substantially elongated (Tables 1 and 2). Note that the bond distances in the optimized geometry of $[\mathbf{2}]^{2-}$ deviate from the crystal structure somewhat more than the ones for the neutral and monoanionic species. In the case of the monoanion, we also optimized the structure with the BP86 functional. The qualitative MO scheme for $[\mathbf{2}]^{2-}$ is shown in Figure 8.

The major difference in the geometric structures of the monoanion and the dianion is the Fe−N−O angle, which changes from essentially linear (175−180°) to bent (145−150°) (Tables 1 and 2). Structures with linear Fe−N−O angles in $[\mathbf{1}]^{2-}$ and $[\mathbf{2}]^{2-}$ have also been located but represent transition states, as indicated by an imaginary frequency with the corresponding transition mode

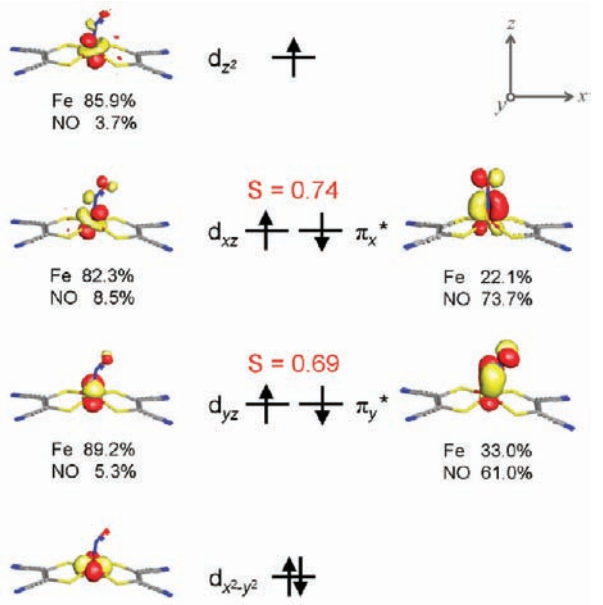

Figure 8. Qualitative MO scheme for $[\mathbf{2}]^{2-}$ from B3LYP DFT calculations. The partial contributions from the Fe, NO, and 2L fragments are shown for selected orbitals.

describing NO bending. The bending of the NO unit is consistent with a NO-centered reduction event, thus leading to a $\{FeNO\}^7$ species.

The electronic structure of $[\mathbf{2}]^{2-}$ calculated with the B3LYP functional (Figure 6) differs from the one predicted by BP86 (Figure S2 of the Supporting Information). The results can be described as follows: (1) Fe(III) (S_{Fe} = $^3/_2$) antiferromagnetically coupled with NO^- (S_{NO} = 1) by B3LYP and (2) Fe(I) (S_{Fe} = $^1/_2$) and NO^+ (S_{NO} = 0) by BP86. The structure of $[\mathbf{2}]^{2-}$ calculated with other functionals (Table S2 of the Supporting Information) shows some variation of the iron and nitrosyl spin populations. Not surprisingly, pure functionals give results similar to BP86, whereas hybrid functionals agree more closely with B3LYP. It is known that, with the higher amount of exact

dx.doi.org/10.1021/ic201565d |*Inorg. Chem.* 2011, 50, 12064–12074

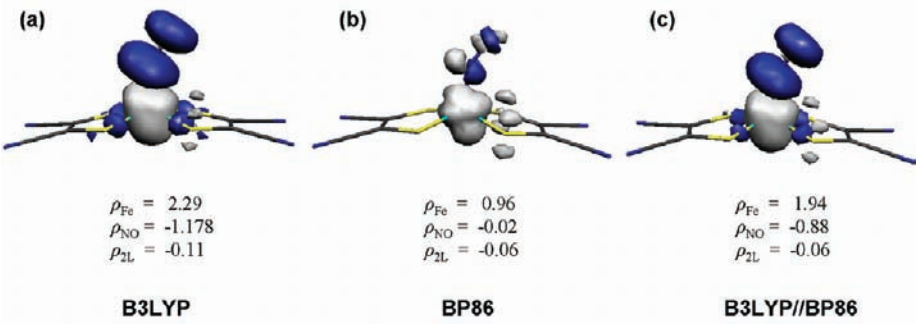

Figure 9. Spin density plots of $[\mathbf{2}]^{2-}$ calculated at the (a) B3LYP, (b) BP86, and (c) B3LYP//BP86 levels of DFT.

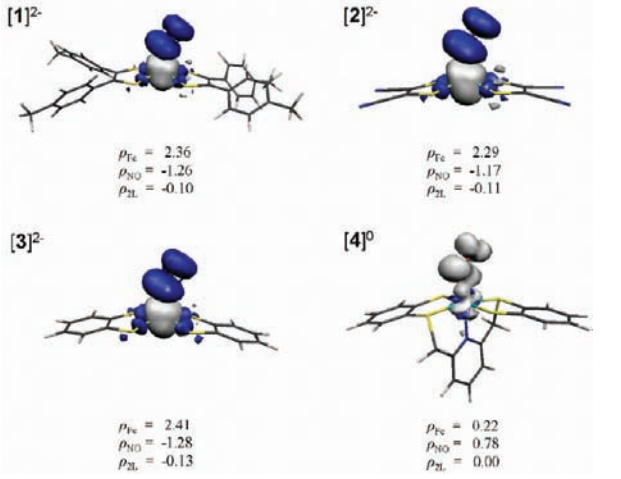

Figure 10. Spin density population analyses for the $\{FeNO\}^7$ complexes: $[\mathbf{1}]^{2-}$, $[\mathbf{2}]^{2-}$, $[\mathbf{3}]^{2-}$, and $[\mathbf{4}]^{0}$, from B3LYP DFT calculations.

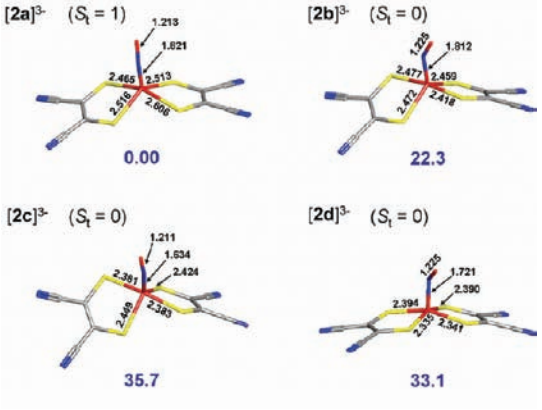

Figure 11. Calculated structures of $[\mathbf{2}]^{3-}$ with energies (kcal mol^{-1}) relative to $[\mathbf{2a}]^{3-}$ denoted in blue. Bond distances are shown in angstrom.

exchange in the functional, high spin states and symmetry breaking is favored.[34,35] In our experience, hybrid functionals are more reliable than pure functionals in most but not all situations.[35] Moreover, the calculated spectroscopic parameters described in the next section all agree with the Fe(III) intermediate spin description. The spin populations calculated with B3LYP at the BP86 optimized structure also support a description of Fe(III) ($S_{Fe} = {}^3/_2$) antiferromagnetically coupled to NO^- (S_{NO} = 1) (Figure 9). The same description holds for $[\mathbf{1}]^{2-}$ (Figure S3 of the Supporting Information).

Related $\{FeNO\}^7$ species with bis-dithiolene ligands ($[Fe(NO)(bdt)_2]^{2-}$, $[\mathbf{3}]^{2-}$ (bdt^{2-} = benzene-1,2-dithiolate),[19] and $[Fe(NO)(pyS_4)]^0$, $[\mathbf{4}]^0$ (pyS_4^{2-} = 2,6-bis(2-mercaptophenylthiomethyl)-pyridine)[36]) were calculated with the B3LYP functional in order to compare them to $[\mathbf{1}]^{2-}$ and $[\mathbf{2}]^{2-}$. As shown in Figure 10, the spin density plots for the five-coordinate complexes, $[\mathbf{1}]^{2-}$, $[\mathbf{2}]^{2-}$, and $[\mathbf{3}]^{2-}$, show positive spin on the Fe and smaller negative spin on the NO fragment. This can be interpreted as Fe(III) ($S_{Fe} = {}^3/_2$) antiferromagnetically coupled to NO^- (S_{NO} = 1). Only the six-coordinate complex, $[\mathbf{4}]^0$, shows positive spin on both the Fe and the NO fragments with a larger amount on the latter, thus suggesting an electronic structure consisting essentially of low spin Fe(II) and $NO^\bullet$ ($S_{NO} = {}^1/_2$), as originally proposed.[36] It is known that for iron-heme type compounds the presence of the sixth ligand shifts the spin density from the iron to the NO ligand.[37]

For the iron bis-dithiolene compounds studied here, the presence of the sixth ligand also affects the electron delocalization between Fe and NO.

f. [Fe(NO)(L_2)]$^{3-}$. The trianion $[\mathbf{2}]^{3-}$ was accessed by electrochemical measurements in previous work,[5] and here we add its infrared spectrum (Figure S5 of the Supporting Information). Several possible structures in singlet and triplet states are calculated for $[\mathbf{2}]^{3-}$ (Figure 11). Two distinct singlet states from spin-unrestricted and spin-restricted calculations were found: (1) $[\mathbf{2c}]^{3-}$, a trigonal bipyramidal structure with a slightly bent Fe−N−O (171.3°), and (2) $[\mathbf{2d}]^{3-}$, a square pyramidal structure with a strongly canted Fe−N−O angle (126.8°). These diamagnetic species are much less stable than $[\mathbf{2a}]^{3-}$ (33.1 and 35.7 kcal mol^{-1}, respectively). The other singlet state, $[\mathbf{2b}]^{3-}$, was calculated with the BS approach and has an electronic structure description of Fe(II) (S_{Fe} = 1) antiferromagnetically coupled to NO^- (S_{NO} = 1). This trigonal bipyramidal dianion with a bent Fe−NO (147.0°) unit is less stable than $[\mathbf{2a}]^{3-}$ by 22.3 kcal mol^{-1}.

The $[\mathbf{2a}]^{3-}$ S_t = 1 species has the lowest energy. The corresponding minimum energy structure resembles a trigonal bipyramid with the NO at the equatorial position and a nearly linear Fe−NO moeity (177.5°). Unlike most $\{FeNO\}^8$ complexes that are diamagnetic,[38] the calculations support a triplet ground state for the trianionic species of **2**. The MO scheme of $[\mathbf{2a}]^{3-}$ (Figure 12) reveals its electronic structure as consisting of Fe(II) (S_{Fe} = 2) antiferromagnetically coupled to NO^- (S_{NO} = 1). Thus, upon reduction of $[\mathbf{2}]^{2-}$, an electron is added to the d_{xy} orbital without

dx.doi.org/10.1021/ic201565d |*Inorg. Chem.* 2011, 50, 12064–12074

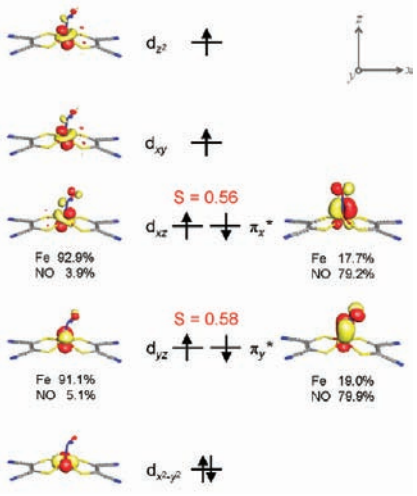

Figure 12. Qualitative MO scheme for $[\mathbf{2a}]^{3-}$ with contributions from the Fe, NO, and 2L fragments noted for selected orbitals.

Table 3. Comparison of Experimental[a] and Calculated Reduction Potentials (V)[b] for 2

	exptl	calcd
$[\mathbf{2}]^{+} + e^{-} \rightarrow [\mathbf{2}]^{0}$		2.09
$[\mathbf{2}]^{0} + e^{-} \rightarrow [\mathbf{2}]^{-}$	0.65	0.63
$[\mathbf{2}]^{-} + e^{-} \rightarrow [\mathbf{2}]^{2-}$	−0.38	−0.17
$[\mathbf{2}]^{2-} + e^{-} \rightarrow [\mathbf{2a}]^{3-}$	−1.83	−1.73

[a] Experimental data shown in Figure S4 of the Supporting Information. [b] Referenced to Fc^{+}/Fc.

a change in the electronic occupation of the NO π^* orbitals which is accompanied by a small structural distortion toward trigonal bipyramidal.

2. Spectroscopic Parameter Calculations of 1 and 2. *a. Reduction Potentials.* Electrochemical studies of $[Fe(NO)(S_2C_2R_2)_2]^z$ complexes showed that R = *p*-tolyl stabilizes more oxidized species while R = CN stabilizes more reduced ones.[4,5] The monocation, which is observed and studied extensively by spectroscopy in series **1**, is not accessible for **2**.[5] On the other hand, the trianion, which is not found for **1**, is detectable in series **2** by cyclic voltammetry, despite the lack of other spectroscopic data.[5]

DFT calculation of the reduction potentials of iron complexes against the ferrocene/ferrocenium (Fc/Fc^{+}) couple have previously yielded reasonable results.[23,39] Here the reduction potentials for the electron transfer series of **2** with solvent correction (in CH_2Cl_2) are calculated to give more support to the assigned electronic structure of $[\mathbf{2}]^{3-}$. The calculated reduction potentials of the $[\mathbf{2}]^{0}/[\mathbf{2}]^{-}$ and $[\mathbf{2}]^{-}/[\mathbf{2}]^{2-}$ redox couples are (Table 3) in good agreement with the experiment. The calculation for $[\mathbf{2}]^{2-}/[\mathbf{2a}]^{3-}$ (−1.73 V) is also consistent with the experimental data (−1.83 V) and, hence, supports the $[\mathbf{2a}]^{3-}$ electronic structure description as an Fe(II) ($S_{Fe} = 2$) ion antiferromagnetically coupled with a triplet NO^{-} ($S_{NO} = 1$). The other proposed electronic structures, $[\mathbf{2b}]^{3-}$, $[\mathbf{2c}]^{3-}$, and $[\mathbf{2d}]^{3-}$, with much higher total energies will clearly yield reduction potentials even more negative than those calculated for $[\mathbf{2a}]^{3-}$.

b. Vibrational Frequencies. The calculated NO stretching frequencies, ν(NO), of the series $[Fe(NO)(L_2)]^z$ are in good agreement with the experimental values (Table 4). The scaling factor of 0.961 is applied for the frequency calculation as suggested by Merrick et al.[40] The ν(NO) values of the neutral and the trianion species of the complex **2**, which were not reported earlier,[5] were also measured in this work (Figure S5 of the Supporting Information). The ν(NO) in **2** is higher than that for the corresponding species in series **1**. This is explained by less π-backbonding from Fe to the nitrosyl, thus resulting in a stronger NO bond. Similar to the experimentally observed trends, the calculated ν(NO) slightly decreases (~20−30 cm^{-1}) along the series for both **1** and **2**. This slight decrease is consistent with a description in which the nitrosyl ligand essentially maintains a NO^{+} state ($S_{NO} = 0$). On the other hand, the calculated ν(NO)

Table 4. Calculated ν(NO) Frequencies for 1 and 2

	calcd	exptl	ref
$[\mathbf{1}]^{+}$	1818	1833	5
$[\mathbf{1}]^{0}$	1799	1800, 1783	5
$[\mathbf{1}]^{-}$	1781	1758	5
$[\mathbf{1}]^{2-}$	1581	1575	5
$[\mathbf{2}]^{+}$	1927		
$[\mathbf{2}]^{0}$	1872	1869	this work
$[\mathbf{2}]^{-}$	1840	1814	5
		1838	this work
$[\mathbf{2}]^{2-}$	1615	1633	5
		1644	this work
$[\mathbf{2a}]^{3-}$	1586	1599	this work
$[\mathbf{2b}]^{3-}$	1488		
$[\mathbf{2c}]^{3-}$	1553		
$[\mathbf{2d}]^{3-}$	1413		

Table 5. Computed δ (mm s^{-1}) and ΔE_Q (mm s^{-1}) Mössbauer Parameters for 1−4 from B3LYP DFT Calculations

	calcd		exptl		
	δ	ΔE_Q	δ	ΔE_Q	ref
$[\mathbf{1}]^{1+}$	0.10	2.00	0.07	1.40	5
$[\mathbf{1}]^{0}$	0.11	1.71	0.06	1.70	5
$[\mathbf{1}]^{-}$	0.01	2.55	0.04	1.88	5
$[\mathbf{1}]^{2-}$	0.37	1.30	0.20	1.16	5
	0.20[a]	0.83[a]			
$[\mathbf{2}]^{1+}$	0.05	2.18			
$[\mathbf{2}]^{0}$	0.06	1.99			
$[\mathbf{2}]^{-}$	0.01	2.53	0.03	1.70	5
			0.05	1.68	41
$[\mathbf{2}]^{2-}$	0.38	1.02	0.33	0.79	5
	0.22[a]	0.65[a]	0.21	0.97	41
			0.28	1.01	this work
$[\mathbf{2}]^{3-}$	0.82	2.62			
$[\mathbf{3}]^{-}$	−0.02	2.79	0.01	2.48	19
$[\mathbf{3}]^{2-}$	0.39	1.27	0.27	1.12	19
	0.22[a]	0.72[a]			
$[\mathbf{4}]^{0}$	0.36	0.50	0.33	0.40	36
	0.29[a]	0.37[a]			

[a] BP86 optimized geometry.

dx.doi.org/10.1021/ic201565d |*Inorg. Chem.* 2011, 50, 12064–12074

Table 6. ^{57}Fe Hyperfine Coupling Parameters (MHz) for $[2]^{2-}$ and $[4]^{0}$

		calcd				exptl				
		A'_x	A'_y	A'_z	A_{iso}	A'_x	A'_y	A'_z	A_{iso}	ref
$[2]^{2-}$	B3LYP//BP86	30.5	−11.3	−19.2	−17.4	25.4	7.8	−33.2	−15.5	this work
	B3LYP	33.6	−13.0	−20.6	−20.8					
$[4]^{0}$	B3LYP	−0.5	−13.1	13.6	5.2	−5.0	13.7	−8.6	−5.6	36

decreases substantially from the monoanion to the dianion for both $[1]^{2-}$ and $[2]^{2-}$ (~200 cm^{-1}), which is consistent with the change in the experimental ν(NO) stretching frequency of ~180−190 cm^{-1}. This is caused by the change of the electronic structure at the nitrosyl ligand to yield NO^{-} (S_{NO} = 1), in which the NO π^* MOs are both occupied.

While the calculated ν(NO) values of the trianions $[\mathbf{2b}]^{3-}$ and $[\mathbf{2d}]^{3-}$ are much too low compared to experiment, good agreement with experiment is found for the calculated ν(NO) of $[\mathbf{2a}]^{3-}$. This result further supports an electronic structure composed of an Fe(II) (S_{Fe} = 2) ion antiferromagnetically coupled with a triplet NO^{-} (S_{NO} = 1). Although the calculated ν(NO) of $[\mathbf{2c}]^{3-}$ could be consistent with experiment, the higher relative energy of $[\mathbf{2c}]^{3-}$ (35.7 kcal mol^{-1}) excludes this possibility. Since the calculated ν(NO) of the trianion is only slightly smaller than the one in the dianion, the same electron occupation in the NO π^* orbitals (NO^{-}, S_{NO} = 1) as found for both $[2]^{2-}$ and $[2]^{3-}$ is apparent.

c. Mössbauer Parameters. The calculated isomer shifts (δ) for the monocation, neutral, and monoanion series of **1** and **2** are in the range of 0.01 to 0.10 mm s^{-1}. The quadruple splitting (ΔE_Q) is in the range of 1.7 to 2.5 mm s^{-1} (Table 5). Both sets of values are in agreement with experiment.[5,19,36,41] Although the experimental isomer shifts of $[1]^{+}$, $[1]^{0}$, and $[1]^{-}$ seem to be insignificantly different (0.04−0.07 mm s^{-1}), the calculated isomer shifts of $[1]^{+}$ and $[1]^{0}$ (~0.10 mm s^{-1}) are noticeably larger than those for $[1]^{-}$ (0.01 mm s^{-1}). This result could be interpreted as indicating some Fe(I) character in $[1]^{+}$ and $[1]^{0}$ but not in the monoanion $[1]^{-}$. This supports an electronic structure composed of {FeNO}^{6} and {FeNO}^{7} resonance forms for $[1]^{+}$ and $[1]^{0}$, and only a {FeNO}^{6} description for $[1]^{-}$. On the other hand, the difference in the isomer shifts of $[2]^{+}$ and $[2]^{0}$ (0.05−0.06 mm s^{-1}) and $[2]^{-}$ (0.01 mm s^{-1}) is less pronounced.

For $[1]^{2-}$, $[2]^{2-}$, and $[3]^{2-}$, the isomer shift significantly increases relative to that of the monoanion (0.20−0.33 mm s^{-1}) and the quadruple splitting drops to about 1.00−1.20 mm s^{-1}. While the Mössbauer calculations at both the BP86 and the B3LYP geometries provide good agreement with the experimental data for six-coordinate $[4]^{0}$, the calculated isomer shifts for the five-coordinate {FeNO}^{7} species ($[1]^{2-}$, $[2]^{2-}$, and $[3]^{2-}$) using the B3LYP optimized structure are significantly overestimated (Table 5). However, the B3LYP derived Mössbauer parameters performed on the BP86 optimized structures are in good agreement with the experimental values. As mentioned earlier, the B3LYP optimized geometry of $[2]^{2-}$ deviates more from the solid state structure than for the BP86 optimized geometry. Lastly, the considerably large isomer shift of 0.82 mm s^{-1} calculated for the {FeNO}^{8} complex $[2]^{3-}$ is typical of a high-spin Fe(II) ion.

The ^{57}Fe hyperfine couplings (HFCs) were calculated for $[2]^{2-}$ and $[4]^{0}$ and compared to the experimental values (Table 6). The spin projection technique[42] is employed for the calculation of the HFCs of $[2]^{2-}$ in the BS state. Although the calculated anisotropic HFCs (A') deviate somewhat from experiment, the isotropic (A_{iso}) values are in good agreement for both $[2]^{2-}$ and $[4]^{0}$. Since BP86 predicts a better geometry for $[2]^{2-}$, the calculated HFCs with B3LYP on the BP86 geometry show a better agreement. Because A_{iso} is directly related to the spin density on the nuclei, the calculated isotropic HFCs support the calculated electronic structures for $[4]^{0}$ and $[2]^{2-}$: (1) a small value of A_{iso} for the six-coordinate $[4]^{0}$ complex corresponds to Fe(II) (S = 0) and NO$^{\bullet}$ ($S = {}^{1}/_{2}$),[36] and (2) a relatively large value of A_{iso} for the five-coordinate $[2]^{2-}$ complex corresponds to Fe(III) ($S_{Fe} = {}^{3}/_{2}$) antiferromagnetically coupled to NO^{-} (S_{NO} = 1).

CONCLUSIONS

The electronic structures of the electron transfer series of $[Fe(NO)(L_2)]^{z}$ (z = 1+, 0, 1−, 2−, 3−) for **1** and **2** were investigated by a combination of spectroscopy and quantum chemistry. The monocationic, neutral, and monoanionic species were previously assigned as {FeNO}^{6} complexes on the basis of the experimental data alone. However, the present study shows that the situation is more complicated. The spectroscopically calibrated calculations reveal that the monocationic and neutral species of **1** are best described by two resonance structures: $\{[Fe^{I}(NO^{+})(L_2^{-})]^{1+} \leftrightarrow [Fe^{II}(NO^{+})(L_2^{2-})]^{1+}\}$ and $\{[Fe^{I}(NO^{+})(L_2^{2-})]^{0} \leftrightarrow [Fe^{II}(NO^{+})(L_2^{3-})]^{0}\}$, respectively, whereas the monoanionic species is indeed best depicted as $[Fe^{II}(NO^{+})(L_2^{4-})]^{-}$ (Scheme 1). On the other hand, only the neutral species of **2** relies on the resonance structure description, while the monocationic and monoanionic species are interpreted as $[Fe^{II}(NO^{+})(L_2^{2-})]^{1+}$ and $[Fe^{II}(NO^{+})(L_2^{4-})]^{-}$, respectively. Although the nitrosyl ligand remains in the NO^{+} oxidation state throughout this redox series, the reduction that mainly changes the bis-dithiolene and/or the iron redox states also weakens the N−O bond through changes in backbonding.

The Fe(I) character seen in some redox species of **1** and **2** is evidenced by an electron occupation of the d_{z^2}-based orbital together with a weak interaction with the dithiolene-based a_1 orbital, and it is observed when the two are at comparable energies. The energy of the a_1 orbital is modulated by the electron withdrawing properties of the substituents (*p*-tolyl/CN) and the oxidation level of the bis-dithiolene ligands, whereas the energy of the Fe d_{z^2}-based orbital of the Fe−NO fragment is more difficult to define because it appears to be influenced by the distance of the Fe ion out of the equatorial 4S plane, which is also affected by the redox level of the chelating dithiolene ligands.

A structure with a canted Fe−NO angle (145−150°) has been calculated for the dianionic {FeNO}^{7} species ($S_t = {}^{1}/_{2}$). Calculated ^{57}Fe isomer shifts and isotropic hyperfine couplings are in a good agreement with the experiment data and support the electronic structure descriptions for both $[1]^{2-}$ and $[2]^{2-}$ as Fe(III) ($S_{Fe} = {}^{3}/_{2}$) antiferromagnetically coupled to NO^{-} (S_{NO} = 1). In contrast to the five-coordinate complexes $[1]^{2-}$, $[2]^{2-}$, and

dx.doi.org/10.1021/ic201565d |*Inorg. Chem.* 2011, 50, 12064–12074

$[3]^{2-}$, the six-coordinate $\{FeNO\}^7$ bis-dithiolene, $[4]^0$, is described as Fe(II) ($S_{Fe} = 0$) and $NO^{\bullet}$ ($S_{NO} = {}^1/_2$).

The calculated NO stretching frequency and the reduction potentials of the electron transfer series of **2** are in agreement with experiment and support a triplet ground state for the $\{FeNO\}^8$ species, $[2]^{3-}$. The calculations suggest that the reduction of the dianion sees one electron added to the empty d_{xy} orbital. Thus, the electronic structure of $[2]^{3-}$ is best viewed as Fe(II) ($S_{Fe} = 2$) antiferromagnetically coupled to NO^- ($S_{NO} = 1$). Unlike most other $\{FeNO\}^8$ species that are diamagnetic with square pyramidal geometries and strongly bent Fe−N−O angles,[38] the formation of $[2]^{3-}$ is only accompanied by a small structural rearrangement consisting of a distortion of the square pyramidal geometry toward a trigonal bipyramid in which the NO ligand occupies an equatorial position and the Fe−N−O angle approaches linearity.

■ ASSOCIATED CONTENT

Supporting Information. Experimental details, cyclic voltammogram, and IR spectra for **2**; applied-field Mössbauer spectra for $[2]^{2-}$; qualitative MO schemes for $[2]^-$, $[2]^{2-}$, and $[1]^{2-}$; and optimized metric parameters and population analyses for computed complexes. This material is available free of charge via the Internet at http://pubs.acs.org.

■ AUTHOR INFORMATION

Corresponding Author

*E-mail: neese@thch.uni-bonn.de (F.N.), wieghardt@mpi-muelheim.mpg.de (K.W.).

Present Addresses

‡Department of Chemistry, Faculty of Science, Mahidol University, 272 Rama VI Road, Ratchathewi, Bangkok 10400, Thailand.

■ ACKNOWLEDGMENT

We thank Drs. Shengfa Ye and Eckhard Bill for helpful discussions, and Dr. Priyabrata Banerjee for preparing a sample of $[NEt_4]_2[2]$. We also thank Prof. James Donahue for providing the crystal structure data for $[2]^{2-}$. P.S. and S.S. are grateful to the Max Planck Society for postdoctoral fellowships. F.N. thanks the Max Planck Society (fellow program) for financial support.

■ REFERENCES

(1) Dithiolene Chemistry: Synthesis, P., and Applications. *Prog. Inorg. Chem.* 2004, *52*, whole volume.
(2) Wang, K.; Stiefel, E. I. *Science* **2001**, *291*, 106.
(3) Yu, R.; Arumugam, K.; Manepalli, A.; Tran, Y.; Schmehl, R.; Jacobsen, H.; Donahue, J. P. *Inorg. Chem.* **2007**, *46*, 5131.
(4) McCleverty, J. A.; Atherton, N. M.; Locke, J.; Wharton, E. J.; Winscom, C. J. *J. Am. Chem. Soc.* **1967**, *89*, 6082.
(5) Ghosh, P.; Stobie, K.; Bill, E.; Bothe, E.; Weyhermüller, T.; Ward, M. D.; McCleverty, J. A.; Wieghardt, K. *Inorg. Chem.* **2007**, *46*, 522.
(6) Sproules, S.; Wieghardt, K. *Coord. Chem. Rev.* **2010**, *254*, 1358.
(7) Enemark, J. H.; Feltham, R. D. *Coord. Chem. Rev.* **1974**, *13*, 339.
(8) Neese, F. *Orca, an Ab Initio, Density Functional and Semiempirical Electronic Structure Program Package*, version 2.8; Universität Bonn: Bonn, Germany, 2010.
(9) (a) Becke, A. D. *J. Chem. Phys.* **1993**, *98*, 5648. (b) Lee, C. T.; Yang, W. T.; Parr, R. G. *Phys. Rev. B* **1988**, *37*, 785. (c) Stephens, P. J.; Devlin, F. J.; Chabalowski, C. F.; Frisch, M. J. *J. Phys. Chem.* **1994**, *98*, 11623.
(10) (a) Becke, A. D. *J. Chem. Phys.* **1988**, *84*, 4524. (b) Perdew, J. P. *Phys. Rev. B* **1986**, *33*, 8822.
(11) Schäfer, A.; Huber, C.; Ahlrichs, R. *J. Chem. Phys.* **1994**, *100*, 5829.
(12) Schäfer, A.; Horn, H.; Ahlrichs, R. *J. Chem. Phys.* **1992**, *97*, 2571.
(13) (a) van Lenthe, E.; Baerends, E. J.; Snijders, J. G. *J. Chem. Phys.* **1993**, *99*, 4597. (b) van Lenthe, E.; Baerends, E. J.; Snijders, J. G. *J. Chem. Phys.* **1994**, *101*, 9783. (c) van Wüllen, C. J. *J. Chem. Phys.* **1998**, *109*, 392.
(14) (a) Pulay, P. *Chem. Phys. Lett.* **1980**, *73*, 393. (b) Pulay, P. *J. Comput. Chem.* **1982**, *3*, 556.
(15) Chatel, S.; Chauvin, A.-S.; Tuchagues, J.-P.; Leduc, P.; Bill, E.; Chottard, J.-C.; Mansuy, D.; Artaud, I. *Inorg. Chim. Acta* **2002**, *336*, 19.
(16) Rae, A. I. M. *Chem. Commun.* **1967**, 1245.
(17) Crystal structure coordinates supplied by Prof. James P. Donahue, Tulane University, New Orleans, LA.
(18) Lee, C.-M.; Hsieh, C.-H.; Dutta, A.; Lee, G.-H.; Liaw, W.-F. *J. Am. Chem. Soc.* **2003**, *125*, 11492.
(19) Lee, C.-M.; Chen, C.-H.; Chen, H.-W.; Hsu, J.-L.; Lee, G.-H.; Liaw, W.-F. *Inorg. Chem.* **2005**, *44*, 6670.
(20) Sellmann, D.; Blum, N.; Heinemann, F. W.; Hess, B. A. *Chem.—Eur. J.* **2001**, *7*, 1874.
(21) Neese, F. *Inorg. Chim. Acta* **2002**, *337*, 181.
(22) (a) Sinnecker, S.; Slep, L.; Bill, E.; Neese, F. *Inorg. Chem.* **2005**, *44*, 2245. (b) Römelt, M.; Ye, S.; Neese, F. *Inorg. Chem.* **2009**, *48*, 784.
(23) Surawatanawong, P.; Tye, J.; Darensbourg, M. Y.; Hall, M. B. *Dalton Trans.* **2010**, *39*, 3093.
(24) Klamt, A.; Schüürmann, G. *J. Chem. Soc., Perkin Trans. 2* **1993**, 799.
(25) Kirchner, B.; Wennmohs, F.; Ye, S.; Neese, F. *Curr. Opin. Chem. Biol.* **2007**, *11*, 134.
(26) (a) Noodleman, L. *J. Chem. Phys.* **1981**, *74*, 5737. (b) Noodleman, L.; Case, D. A.; Aizman, A. *J. Am. Chem. Soc.* **1988**, *110*, 1001. (c) Noodleman, L.; Davidson, E. R. *Chem. Phys.* **1986**, *109*, 131. (d) Noodleman, L.; Norman, J. G.; Osborne, J. H.; Aizman, A.; Case, D. A. *J. Am. Chem. Soc.* **1985**, *107*, 3418. (e) Noodleman, L.; Peng, C. Y.; Case, D. A.; Monesca, J. M. *Coord. Chem. Rev.* **1995**, *144*, 199. (f) Chłopek, K.; Muresan, N.; Neese, F.; Wieghardt, K. *Chem.—Eur. J.* **2007**, *13*, 8390.
(27) Neese, F. *J. Phys. Chem. Solids* **2004**, *65*, 781.
(28) (a) Hall, M. B.; Fenske, R. F. *Inorg. Chem.* **1972**, *11*, 768.(b) Manson, J.; Webster, C. E.; Pérez, L. M.; Hall, M. B. *Jimp 2*. http://www.chem.tamu.edu/jimp2/index.html.
(29) *Molekel*, Advanced Interactive 3D-Graphics for Molecular Sciences; Swiss National Supercomputing Center: http://www.cscs.ch/molkel.
(30) Neese, F. *Coord. Chem. Rev.* **2009**, *253*, 526.
(31) Neese, F. *J. Biol. Inorg. Chem.* **2006**, *11*, 702.
(32) Ray, K.; Weyhermüller, T.; Neese, F.; Wieghardt, K. *Inorg. Chem.* **2005**, *44*, 5345.
(33) (a) Linder, D. P.; Rodgers, K. R.; Banister, J.; Wyllie, G. R. A.; Ellison, M. K.; Scheidt, W. R. *J. Am. Chem. Soc.* **2004**, *126*, 14136. (b) Linder, D. P.; Rodgers, K. R. *Inorg. Chem.* **2005**, *44*, 1367.
(34) (a) Daku, L. M. L.; Vargus, A.; Hauser, A.; Fouqueau, A.; Casida, M. E. *Chem. Phys. Chem.* **2005**, *6*, 1393. (b) Reiher, M.; Salomon, O.; Hess, B. A. *Theor. Chem. Acc.* **2001**, *107*, 48.
(35) Ye, S.; Neese, F. *Inorg. Chem.* **2010**, *49*, 772.
(36) Li, M.; Bonnet, D.; Bill, E.; Neese, F.; Weyhermüller, T.; Blum, N.; Sellmann, D.; Wieghardt, K. *Inorg. Chem.* **2002**, *41*, 3444.
(37) Praneeth, V. K. K.; Neese, F.; Lehnert, N. *Inorg. Chem.* **2005**, *44*, 2570.
(38) (a) Pellegrino, J.; Bari, S. E.; Bikiel, D. E.; Doctorovich, F. *J. Am. Chem. Soc.* **2009**, *132*, 989. (b) Serres, R. G.; Grapperhaus, C. A.; Bothe, E.; Bill, E.; Weyhermüller, T.; Neese, F.; Wieghardt, K. *J. Am. Chem. Soc.* **2004**, *126*, 5138.
(39) (a) Fu, Y.; Liu, L.; Yu, H.-Z.; Wang, Y.-M.; Guo, Q.-X. *J. Am. Chem. Soc.* **2005**, *127*, 7227. (b) Holland, J. P.; Green, J. C.; Dilworth, J. R. *Dalton Trans.* **2006**, 783. (c) Moens, J.; Geerlings, P.; Roos, G.

Chem.—Eur. J. **2007**, *13*, 8174. (d) Patterson, E. V.; Cramer, C. J.; Truhlar, D. G. *J. Am. Chem. Soc.* **2001**, *123*, 2025.

(40) Merrick, J. P.; Moran, D.; Radom, L. *J. Phys. Chem. A* **2007**, *111*, 11683.

(41) Birchall, T.; Greenwood, N. N. *J. Chem. Soc. A* **1969**, 286.

(42) (a) Orio, M.; Pantazis, D.; Petrenko, T.; Neese, F. *Inorg. Chem.* **2009**, *48*, 7251. (b) Pantazis, D.; Orio, M.; Petrenko, T.; Zein, S.; Bill, E.; Lubitz, W.; Messinger, J.; Neese, F. *Chem.—Eur. J.* **2009**, *15*, 5108. (c) Schäfer, K.-O.; Bittl, R.; Zweygart, W.; Lendzian, F.; Haselhorst, G.; Weyhermüller, T.; Wieghardt, K.; Lubitz, W. *J. Am. Chem. Soc.* **1998**, *120*, 13104. (d) Sinnecker, S.; Neese, F.; Noodleman, L.; Lubitz, W. *J. Am. Chem. Soc.* **2004**, *126*, 2613.